




Electrocatalytic oxidation of methanol, ethylene glycol and glycerine in alkaline media on TiO₂ nanotubes decorated with AuCu nanoparticles for an application in fuel cells

Wiktoria Lipińska^{1,*} , Katarzyna Grochowska¹, Jakub Karczewski^{2,3}, Emerson Coy⁴, and Katarzyna Siuzdak¹

¹Centre for Plasma and Laser Engineering, The Szewalski Institute of Fluid-Flow Machinery Polish Academy of Sciences, Fiszerza 14 St, 80-231 Gdańsk, Poland

²Institute of Nanotechnology and Materials Engineering, Faculty of Applied Physics and Mathematics, Gdańsk University of Technology, Narutowicza 11/12 St, 80-233 Gdańsk, Poland

³Advanced Materials Center, Gdańsk University of Technology, Narutowicza 11/12 St, 80-233 Gdańsk, Poland

⁴NanoBioMedical Centre, Adam Mickiewicz University, Wszechnicy Piastowskiej 3, 61-614 Poznań, Poland

Received: 31 January 2022

Accepted: 22 June 2022

Published online:
14 July 2022

© The Author(s), under exclusive licence to Springer Science+Business Media, LLC, part of Springer Nature 2022

ABSTRACT

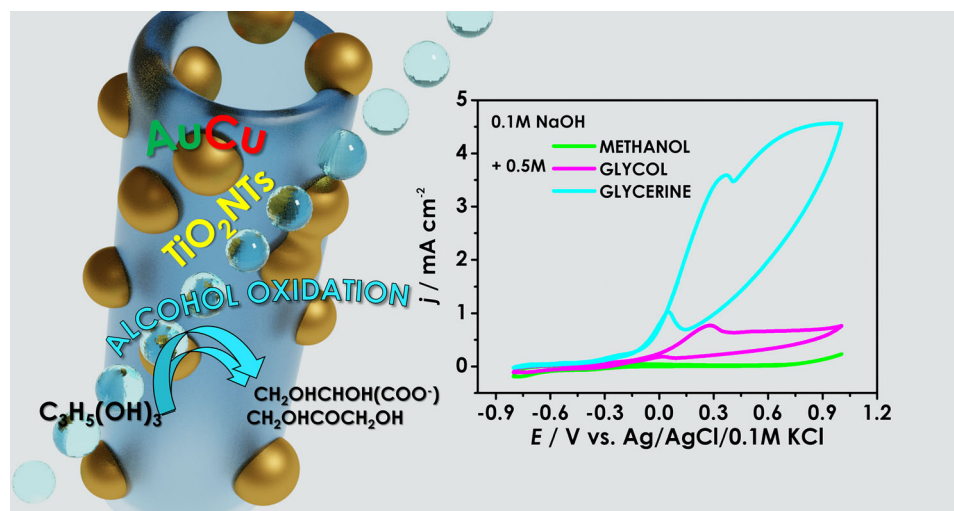
In this work, we present the catalytic and photocatalytic activity of AuCu nanostructures obtained on TiO₂ nanotubes toward methanol, ethylene glycol and glycerine oxidation. The electrode material is prepared by anodization of Ti foil, thin AuCu layer sputtering and rapid thermal treatment under argon atmosphere. Scanning electron microscopy images confirmed the presence of ordered tubular architecture of TiO₂ as well as nanoparticles formed on the surface of the nanotubes. The electrodes were measured using cyclic voltammetry, linear voltammetry and electrochemical impedance spectroscopy in dark and under illumination. Obtained results show a significant current increase: 20 and 90 times higher current density at + 0.3 V versus Ag/AgCl/0.1 M KCl after glycol and glycerine addition, respectively. Moreover, a higher current toward alcohol oxidation was registered for thermally annealed samples than for non-annealed ones. Reported studies demonstrate deep insight into the electrical properties of AuCu-modified titania materials.

Handling Editor: Christopher Blanford.

Address correspondence to E-mail: wlipinska@imp.gda.pl

<https://doi.org/10.1007/s10853-022-07471-7>

GRAPHICAL ABSTRACT



Introduction

Non-renewable energy fuels represent most of the contribution to the world energy production. Raw materials have a limited amount; their extraction and exploitation result in the Earth balance disability and its destruction. It can be seen as climate changes and ecosystem disturbance.

Therefore, nowadays novel energy conversion devices are extremely significant. First fuel cell was discovered 180 years ago and has become extensively studied since that days because of its more environmentally friendly properties than conventional energy sources such as coal or gas [1]. Such devices allow to convert chemical energy into electrical one without pollutant gasses emission [2]. As a fuel, one can distinguish hydrogen [3], methane [4] or alcohol such as methanol, ethanol, glycol and glycerine.

The study of alcohol electrooxidation is of major importance for fuel and electrolytic cells used as a power generation source. Furthermore, the alkaline electrolyte used in those devices can offer a number of advantages comparing to acidic media, such as improved kinetics at both anode and cathode for alcohol oxidation, reduced adsorption of spectator ions as well as lower corrosion rate [5]. The commercial electrodes used in cells are based on Pt plate

[6], and therefore, the alternative and economic electrocatalytic materials for alcohol oxidation are of increasing urgency. The Pt catalyst can be replaced with bimetallic gold–copper metallic nanoparticles (NPs) or AuCu NPs supported on platform material which improves their catalytic activity, stability as well as influences on dispersion and size distribution of NPs [7, 8].

In recent years, bimetallic NPs have attracted increasing attention in view of synergistic effect which triggers unique chemical and physical properties of nanoparticles. The bimetallic NPs can be produced by many advanced synthetic methods which allow to control their size, shape, crystal structure and composition [9]. Various morphologies and compositions can enhance catalytic activity of nanoparticles. As far as copper is concerned, it plays a prominent part in improvement of catalytic activity for noble metal such as Au, Pt and Pd owing to weaker strength of metal–CO bonds and better regeneration of active sites [10]. Especially, AuCu NPs are widely used for alcohol oxidation [10, 11] such as methanol, ethanol, glycol, glycerine, benzyl alcohol as well as CO [12] or H₂O₂ [13] oxidation. According to Sobczak and Wolski [14], the AuCu system based on Nb₂O₅ was active toward methanol and glycerol oxidation processes. The addition of copper to Au–Nb₂O₅ increases the activity in contrast

to monometallic gold electrode. Copper which was present in the form of CuO, oligonuclear $[\text{Cu}^{\delta+} \cdots \text{O}^{\delta-} \cdots \text{Cu}^{\delta+}]_n$ clusters and isolated cations, led to changes in the chemical nature of gold resulting in increase in metallic gold content. Moreover, Biswas et al. [15] investigated more efficient methanol oxidation reaction on the AuCu bimetallic nanostructures than on their monometallic counterparts. Furthermore, Palacio et al. [16] converted glycerol in aqueous media at high reaction temperature of 200 °C on the AuCu/CeO₂ catalyst and showed that copper improved gold activity owing to higher selectivity and longer catalytic lifetime. Apart from pure catalytic processes, also photocatalytic oxidation of alcohols is strongly developed field [17] since the process can be supported by the solar radiation. Then photons are responsible for initiation of the chemical reaction on metal/semiconductor interface [17] in contrast to electrocatalysis where metal active sites are responsible for it. Higher photocatalytic activity resulting from light harvesting in visible light and promotion of charge separation is facilitated by surface plasmon resonance of Au and Cu NPs [18]. According to Chen et al. [18], AuCu@CeO₂ bimetallic-core CeO₂ shell nanocomposite exhibits high activity toward benzyl alcohol photocatalytic oxidation. Furthermore, the Cu species improve the catalytic oxidation via AuCu alloy and oxygen vacancy formation. The AuCu NPs can be fabricated using bottom-up or top-down methods. The synthesis of such nanoparticles by bottom-up technique can be performed using H₂AuCl₄·H₂O and Cu(CH₃COO)₂·H₂O liquid solutions with heating at the temperatures in the range of 80–300 °C [19]. As an example of top-down method, Au and Cu magnetron sputtering with further heating up to ca. 300 °C in Ar or N₂ atmosphere can be performed [20].

In our work, we present the properties of gold-copper-modified titania nanotubes (TiO₂NTs) fabricated via electrochemical anodization of Ti foil, thin AuCu layers magnetron sputtering and rapid thermal annealing (RTA) in argon atmosphere. Nanomaterials morphology was characterized using scanning and transmission electron microscopy (SEM, TEM) techniques. The electrocatalytic and photocatalytic activities were tested toward methanol, ethylene glycol and glycerine oxidation. The electrochemical measurements were carried out in 0.1 M NaOH solution containing alcohol using cyclic voltammetry (CV), linear voltammetry (LV) and

electrochemical impedance spectroscopy (EIS) in dark and under visible light electrode illumination. It should be highlighted that, attention has been also paid to the comparison between catalytic efficiency of non-annealed and annealed bimetallic electrodes. Thermally treated materials have larger active surface and more active sites used for alcohol oxidation. As it was expected, thermal treatment strongly influences on stability and activity of fabricated materials.

Experimental

Materials

Titanium foil (99.7%, Strem), acetone (99.5%, Chempur), ethanol (96%, Chempur), ammonium fluoride (Chempur), diethylene glycol (99.5% Chempur), hydrofluoric acid (Chempur) were used for the electrochemical anodization process. The AuCu target (Au50/Cu50 At%, Goodfellow) and targets of gold (99.99%, Quorum Technologies) and copper (99.99%, Quorum Technologies) were exploited for metal layer deposition. The Ar gas (Air Liquide Polska Sp. z o o.) was used for thermal annealing as well as electrolyte deaeration. NaOH (P.P.H “STANLAB” Sp. J), methanol (ME, 99.8%, POCH), ethylene glycol (GE, 99.5%, Chempur), glycerine (GLY, POCH) were used for electrochemical measurements.

Electrode fabrication

Firstly, the Ti foil was cut into 2 × 3 cm² plates and ultrasonically cleaned in acetone, ethanol and water for 10 min. Titania nanotubes were fabricated via electrochemical anodization process in a two-electrode system, where Ti was an anode and Pt mesh was used as a cathode. The electrolyte contained 0.09 M NH₄F/1.3% vol. HF/6.2% vol. H₂O/92.5% vol. diethylene glycol. The anodization was carried out in thermostated glass cell at the temperature of 40 °C and the voltage of 30 V for 2 h. After anodization TiO₂ nanotubes were rinsed with ethanol and dried in cold air. Secondly, nanotubes were covered by thin 10 nm thick AuCu alloy layer by magnetron sputtering (Q150T S system, Quorum Technologies). Samples which were fabricated up to this step are labeled as n-ACT. Next electrodes were thermally treated in a Rapid Thermal Annealing

furnace (MILA 5000 P-N) at 450 °C for 1 h in argon atmosphere. TiO₂ nanotubes modified by AuCu alloy and annealed in RTA are assigned as an-ACT. Moreover, as a reference sample pure TiO₂ nanotubes were thermally treated also in the same conditions and an-ACT was used as their label. The applied fabrication procedure for monometallic electrodes consisted of electrochemical anodization of Ti plate, magnetron sputtering of thin 5 nm Au or Cu layers and thermal treatment also (assigned as an-AT and an-CT, respectively).

Samples characterization

The morphology and cross section of the samples were investigated by the field emission scanning electron microscope (FEI Quanta FEG250) equipped with an ET secondary detector and with the beam accelerating voltage kept at 10 kV. The nanotubes and nanoparticles size was analyzed by Gwyddion. The an-ACT sample was measured in aberration-corrected high-resolution transmission electron microscope (JEOL ARM 200F) equipped with an EDX (energy-dispersive X-ray) detector. Measurements were performed at an accelerating voltage of 200 eV. The electrochemical and photoelectrochemical measurements of pure and modified nanotubes were conducted using potentiostat–galvanostat system (AutoLab PGStat 302 N) in three-electrode arrangement, where TiO₂NTs, n-ACT and an-ACT served as working electrodes (WE), Pt mesh as counter electrode (CE) and Ag/AgCl/0.1 M KCl as a reference electrode (RE). All electrochemical measurements were carried out in deaerated 0.1 M NaOH solution and 0.1 M NaOH with 0.5 M methanol, 0.5 M ethylene glycol or 0.5 M glycerine. Cyclic and linear voltammetry curves were registered from -0.8 V to +1 V with a scan rate of 50 mV/s and 10 mV/s, respectively. LV scans under visible light illumination were measured using xenon lamp (LOT-QuantumDesign GmbH). Electrochemical impedance spectroscopy measurements were conducted for an-ACT sample at frequency from 20 kHz to 0.1 Hz covering 20 points per decade and with 0.01 V amplitude at the open circuit potential (OCP) in dark and during electrode illumination. The impedance data were analyzed on the basis of an electrical equivalent circuit (EEQC) via EIS Spectrum Analyser.

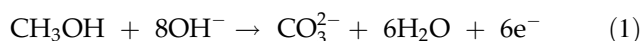
Results and discussion

Morphology

Figure 1 shows the morphology of the pure titania nanotubes and nanotubes modified by gold–copper nanoparticles. The diameter of TiO₂NTs is equal to 101 ± 13 nm and the wall thickness to 13 ± 3 nm. Moreover, cross section image of nanotubes allows the determination of length: 709 ± 53 nm. Nanotubes were covered by thin AuCu layer using magnetron sputtering resulting in increase in wall thickness up to 20 ± 4 nm. After thermal treatment spherical gold–copper nanoparticles with a diameter of 38 ± 5 nm were formed on the NTs surface. The AuCu NPs are present in the crown position [21] as well as on nanotubes walls. The TEM images showed that particles are consistently bigger at the top of the TiO₂ nanotubes (Fig. 2). The diameter changes from ca. 60 to ca. 5 nm. EDX images allow to confirm the presence of AuCu nanoparticles and their distribution mostly in the upper part of nanotubes. The thorough studies of other physicochemical properties of prepared material can be found in our previous work [22].

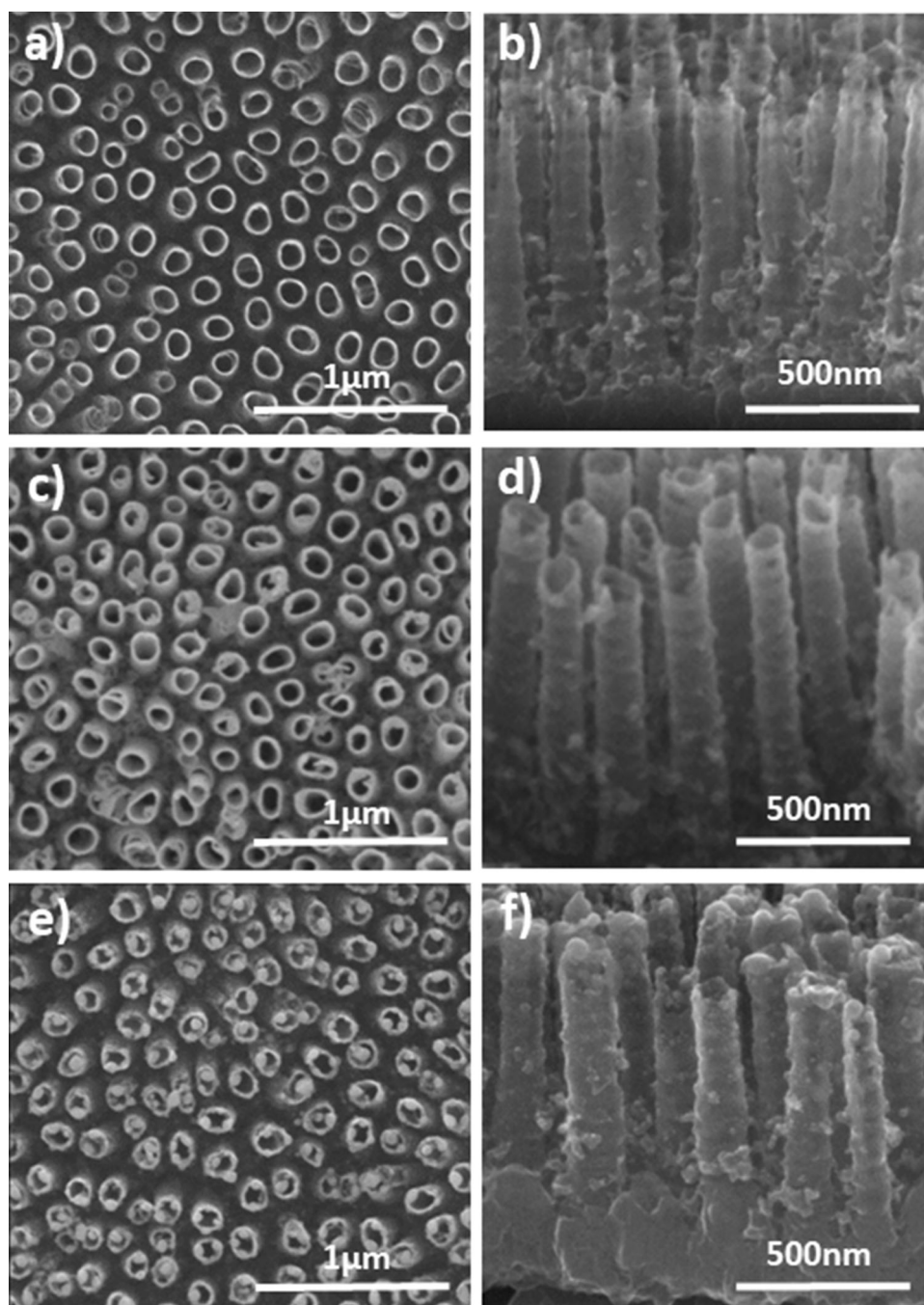
Electrochemical performance

The electrochemical activity toward alcohol electrooxidation of non-annealed and annealed ACT as well as TiO₂NTs electrodes was characterized using cyclic voltammetry. In this work, the measurements were carried out in 0.1 M NaOH solution containing methanol, ethylene glycol or glycerine with a concentration of 0.5 M. The results are shown in Fig. 3. The reactions of alcohol electrooxidation in alkaline media (1–3) consume OH⁻ depending on the number of hydroxyl groups per molecule. The number of electrons captured can be different:



The number of electrons indicates the available amount of energy accumulated in particular alcohol [23] for further utilization toward energy conversion and storage. After the addition of methanol, no intense peaks related to the alcohol oxidation were observed (Fig. 3a). Moreover, capacitance currents

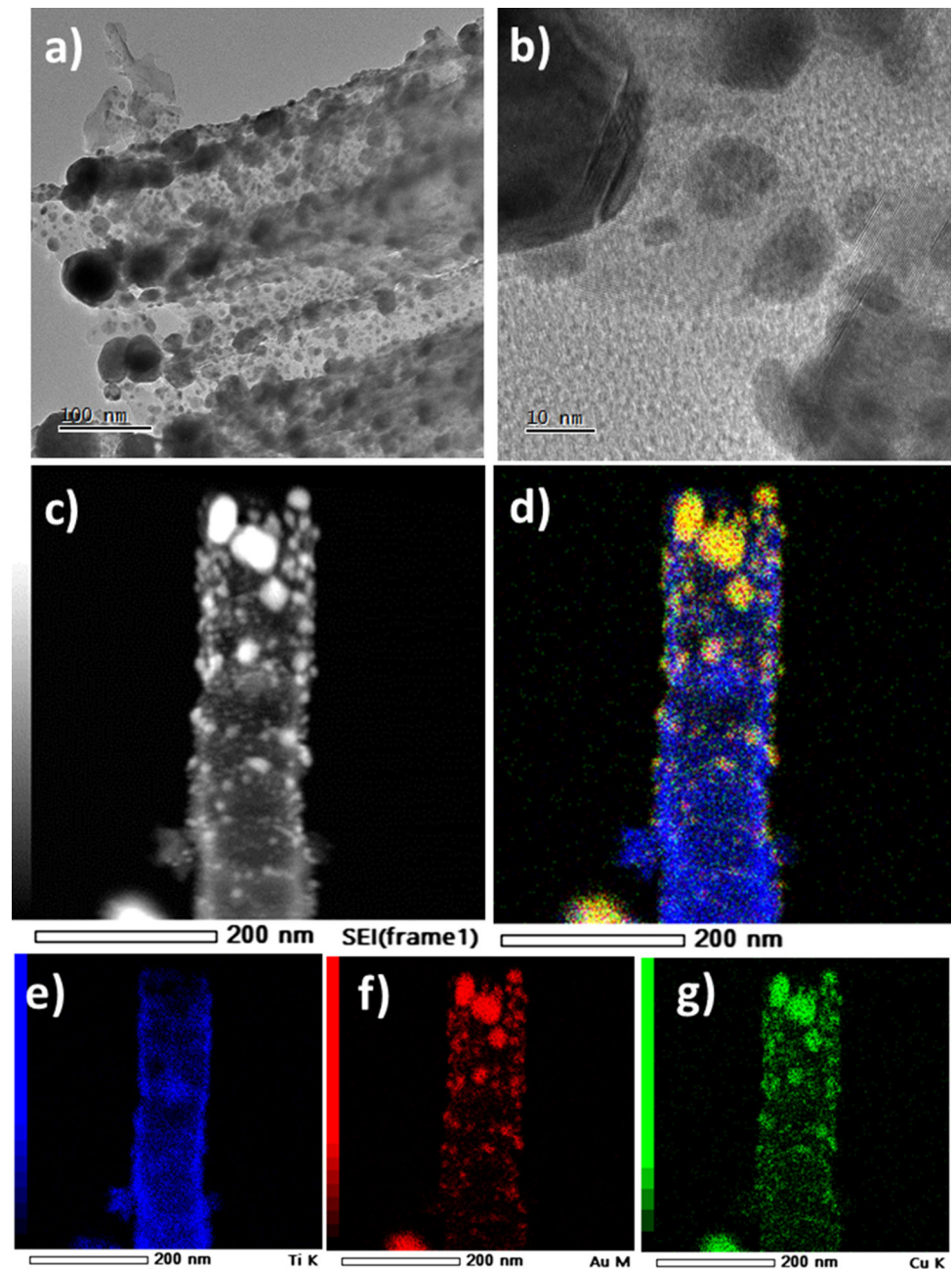
Figure 1 SEM images of **a** TiO₂NTs, **b** cross section of TiO₂NTs, **c** n-ACT, **d** cross section of n-ACT, **e** an-ACT and **f** cross section of an-ACT [22].



densities from -0.8 V to $+0.1$ V were lower in the 0.5 M methanol solution comparing to 0.1 M NaOH, especially for the an-ACT electrode for the reduction peaks at -0.8 V and -0.5 V as well as the oxidation peaks at -0.2 V and $+1$ V versus Ag/AgCl/ 0.1 M KCl. Therefore, the TiO₂NTs, n-ACT and an-ACT materials do not enable electrocatalytic methanol oxidation. According to Biswas et al. [15] pure Cu, Au or Au/Cu nanoparticles exhibited activity for the

methanol oxidation at the potential of $+0.55$ V, $+0.52$ V and $+0.46$ V versus Ag/AgCl in 0.5 M methanol solution. The X-ray photoelectron spectroscopy measurements confirmed metallic states of Au located at 83.67 eV and Cu at 932.77 eV in the Au/Cu nanostructure and absence of oxide species [22]. However, in our case, for the an-ACT electrode thermally treated in argon four copper and two gold separate chemical states were identified [22].

Figure 2 a, b TEM and c–g EDX images of an-ACT electrode.



Additionally, CuAuTi , AuCu , CuO , Cu(OH)_2 , $\times \text{CuCO}_3$ and Au_2O were present on the electrode surface. It can indicate that formation of oxides decreases materials activity toward methanol oxidation due to the less-exposed surface atoms of Au and Cu. In the case of ethylene glycol, the oxidation process takes place both for non-annealed AuCu electrode as well as annealed AuCu sample (Fig. 3b). The proposed oxidation mechanism of $\text{C}_2\text{H}_4(\text{OH})_2$ can be found in the literature [24–27]. The ethylene glycol can be oxidized to oxalate $(\text{COO}^-)_2$, formate

(HCOO^-) or carbonate (CO_3^{2-}) . Two intense anodic peaks located at +0.3 V and +1 V versus Ag/AgCl/0.1 M KCl can be found for the an-ACT electrode, whereas for the n-ACT sample the second peak is shifted by -0.25 V. The anodic current density registered at +0.3 V for the annealed AuCu material increases from ca. $40 \mu\text{A cm}^{-2}$ to $800 \mu\text{A cm}^{-2}$ after the ethylene glycol addition while at +1 V the value enhances from ca. $300 \mu\text{A cm}^{-2}$ to $800 \mu\text{A cm}^{-2}$. The current density due to the glycol oxidation registered at +0.3 V is 2 times higher for thermally treated

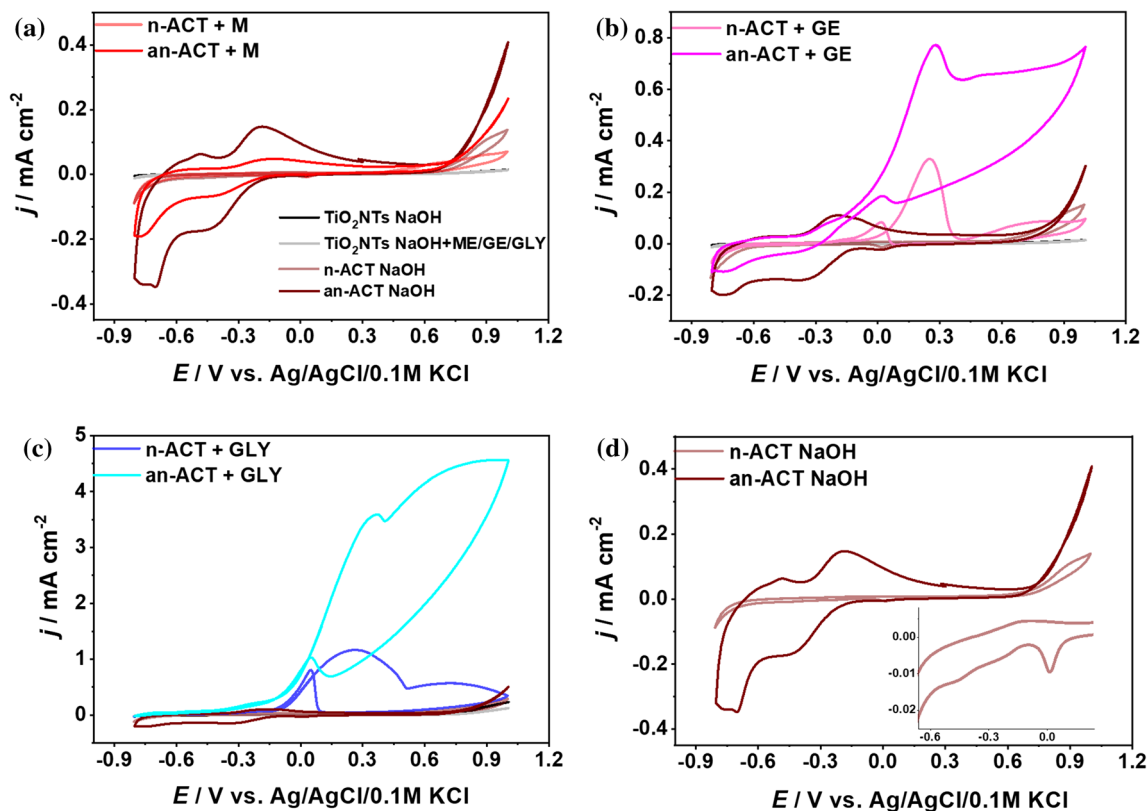


Figure 3 Cyclic voltammograms for TiO_2NTs , n-ACT and an-ACT electrodes in 0.1 M NaOH with or without 0.5 M: **a** methanol, **b** ethylene glycol, **c** glycerine and **d** 0.1 M NaOH.

bimetallic electrode than for the non-annealed one. Moreover, the value of current density at +1 V is about 8 times higher for the an-ACT electrode than for the n-ACT sample. As for the ACT sample fabricated using the RTA furnace, the electrocatalytic activity toward glycol oxidation is much more intensive than for materials without the thermal treatment which is caused by the larger electrochemical active surface area and a greater amount of active sites [28]. Besides, it should be evoked here that TiO_2NTs alone are not sensitive to glycol. According to Marelli et al. [9], the highest activity toward benzyl alcohol oxidation with respect to Au monometallic electrode was achieved for sample containing low amount of CuO oxide which partially covers the Au-rich core of the NPs that indicated that the synergistic effect occurs. Whereas, when the CuO completely covers the AuNPs, the reaction is inhibited. It should be highlighted that the catalysis process takes place on Au and Cu metallic components while Cu_2O , CuO or TiO_2 semiconductors are regarded here only as the catalyst support [29]. According to Fashedemi et al. [30], the FeCo@Fe@Pd/C

electrode has shown activity in the electrooxidation of ethylene, ethylene glycol and glycerol. The current densities of ca. 4 mA cm^{-2} , 5 mA cm^{-2} , 4.8 mA cm^{-2} at 0 V versus Ag/AgCl/KCl were registered in 0.5 M KOH with 0.5 M ethanol, GE and GLY, respectively. Therefore, the palladium-based material exhibits the best electrocatalytic performance toward ethylene glycol. In our work, the AuCu electrodes are electrocatalytically active both toward glycol and glycerine. The CV scans recorded in alkaline solution with 0.5 M glycerine are shown in Fig. 3c. The peaks located at +0.3 V and +1 V correspond to $\text{C}_3\text{H}_5(\text{OH})_3$ oxidation process [31]. The proposed mechanism can be found in the literature [24, 26, 27], where two various intermediates are possible to be formed during reaction such as glyceric acid $\text{CH}_2\text{OHCHOH}(\text{COO}^-)$ and dihydroxyacetone $\text{CH}_2\text{OHCOCH}_2\text{OH}$. Similarly as for ethylene glycol reaction oxalate, formate and carbonate might be the final products. The significant enhancement of the current density from $38 \mu\text{A cm}^{-2}$ to 3.6 mA cm^{-2} is recorded for the an-ACT sample at +0.3 V versus Ag/AgCl/0.1 M KCl after glycerine addition to the

electrolyte. When the electrode is polarized toward more anodic direction the current increase from $505 \mu\text{A cm}^{-2}$ to even 4.56 mA cm^{-2} at + 1 V is observed. The materials annealed at the RTA furnace exhibit improved activity toward glycerine oxidation than non-annealed ones. The current density of alcohol oxidation was 3 or even 11 times higher at + 0.3 V and + 1 V, respectively. Such improvement was reported by Houache et al., [32] for Ni electrode that was electrochemically treated in the solution of 0.1 M Na_2SO_4 with 30 mM ascorbic acid and 4 times higher current density for glycerol electrooxidation was noted than for the untreated sample. Such behavior was justified by the formation of active sites of nickel oxyhydroxide where catalytic reaction takes place. In the case of our material, we regard that similar phenomena take place. Moreover, we should take into account the CuAuTi alloy which is present only at the an-ACT material [22]. As far as the TiO_2NTs electrode is concerned, no electrocatalytic activity toward glycerine was registered.

Figure 3d presents electrochemical response for n-ACT and an-ACT electrodes registered in 0.1 M NaOH solution. The intense faradic peaks can be observed for the thermally treated sample in contrast to non-annealed material with only one reduction peak located at ca. 0 V which may correspond to reduction of gold oxides [33]. According to Liu et al. [34], unidirectional diffusion from the Au shell to Cu core was explored via thermal alloying. The core-shell samples were heated up to 260 °C finally forming AuCu intermetallic compound. Therefore, various shapes of CVs curves are observed resulting from different internal structures of bimetallic AuCu compounds that underwent change during thermal treatment. For the an-ACT electrode, two anodic and two cathodic peaks associated with copper oxides redox reactions can be distinguished [35]. It can be claimed that two-stage oxidation process of Cu to CuO and reduction of CuO to Cu can be observed for this material [36]. The CV scans correlate with the XPS data for an-ACT electrode where copper was detected in two forms such as metallic Cu (CuAuTi, AuCu) as well as copper (II) oxides [22].

The cyclic voltammetry curves for Au and Cu deposited on TiO_2NTs registered in alkaline solution without and with 0.5 M methanol, ethylene glycol or glycerine are shown in Fig. 4. In the case of methanol, after its addition to the solution no oxidation peak can be observed (Fig. 4a). For ethylene glycol, the

oxidation takes place only on gold-modified electrode (Fig. 4b). One oxidation peak at + 1 V versus Ag/AgCl/0.1 M KCl can be distinguished for the an-AT electrode, whereas for the bimetallic AuCu electrodes two anodic peaks located at + 0.3 V and + 1 V were observed. The addition of copper to gold nanoparticles is responsible for synergistic effect and formation of second oxidation peak at lower potentials. Taking into account current density at + 0.3 V for the an-AT electrode its value increased from 23 to $408 \mu\text{A/cm}^2$ which is two times lower than for bimetallic an-ACT electrode at the same potential. This behavior confirmed the positive effect of the alloy on the catalytic activity toward ethylene glycol oxidation providing reduction of oxidation potential as well as increase in current density. In the case of glycerine, the activity was also obtained only for gold-modified electrode (Fig. 4c). Here, also only one oxidation peak can be found for the an-AT electrode at + 0.6 V. However, current density recorded at + 0.3 V for the an-AT electrode is 2.5 times higher than for AuCu bimetallic samples.

In order to evaluate the photoactivity of the fabricated nanomaterials, the linear voltammetry measurements in dark and under vis illumination were carried out (Fig. 5). The LV scans were recorded in 0.1 M NaOH and in 0.1 M NaOH with 0.5 M methanol, ethylene glycol or glycerine solution. The n-ACT electrode measured in 0.1 M NaOH as well as with methanol does not show any photocurrent growth, moreover the decrease in current density during illumination can be seen above + 0.75 V versus Ag/AgCl/0.1 M KCl (Fig. 5a). This activity can result from the presence of amorphous TiO_2 in contrast to thermally treated samples. As far as the an-ACT sample is concerned, where TiO_2NTs are present in the crystalline form [22], the addition of methanol caused the increase in photoactivity in the range from - 0.5 V to + 0.8 V (Fig. 5b). It should be highlighted that the presence of bimetallic AuCu structures has got significant effect on LVs results obtained in methanol solution. As it was described above, materials which contain gold and copper are electroactive, namely the oxidation of ethylene glycol and glycerine occurs at their surface. Not only above presented reactions take place but also radical-catalyzed alcohol oxidation by photogenerated holes (photocatalytic activity). According to our earlier work [22], the positive photocurrent spikes for the structures containing AuCu were observed from

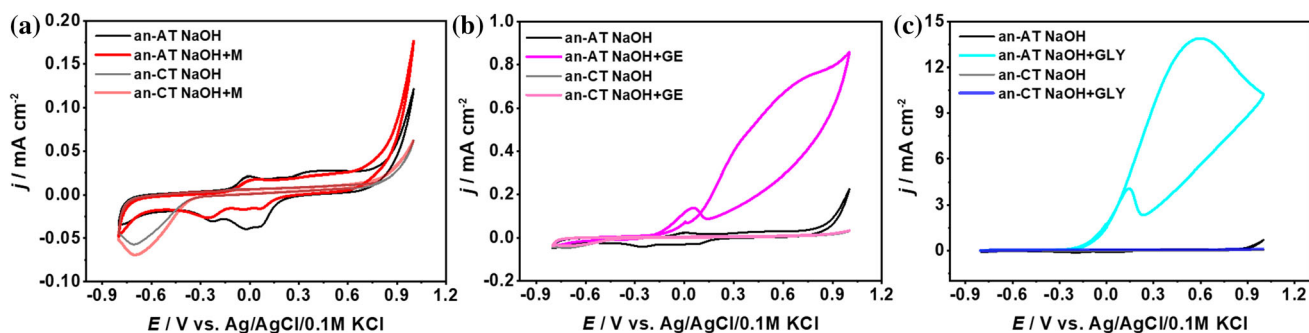


Figure 4 Cyclic voltammetry curves for an-AT and an-CT electrodes in 0.1 M NaOH with or without 0.5 M: **a** methanol, **b** ethylene glycol and **c** glycerine.

– 0.8 to + 0.6 V when the electrode is exposed to light. The mechanism of ethylene glycol oxidation by photogenerated holes is shown in Scheme 1 [37–39].

The electron–hole pairs are generated on TiO_2 , Cu_2O and CuO , sequentially holes which come from copper oxides are consumed in the photocatalytic alcohol oxidation. For the n-ACT electrode, the enhancement of current density from $67 \mu\text{A cm}^{-2}$ to $277 \mu\text{A cm}^{-2}$ at ca. + 0.3 V in ethylene glycol solution was achieved during light illumination (Fig. 5c). The increase in photocurrent above – 0.3 V versus Ag/AgCl/0.1 M KCl was registered for the an-ACT sample immersed in 0.1 M NaOH with 0.5 M $\text{C}_2\text{H}_4(\text{OH})$ (Fig. 5d) due to the activity of AuCu annealed at 450 °C in argon atmosphere. Besides, the current grows from 0.5 mA cm^{-2} to 0.73 mA cm^{-2} at the potential of ca. + 0.3 V. The values of photocurrent density defined as the difference between current recorded under illumination and in dark obtained for the non-annealed electrode and the annealed one are quite similar and are equal to $210 \mu\text{A cm}^{-2}$ and $230 \mu\text{A cm}^{-2}$ at + 0.3 V, respectively (Table 1). Therefore, it may be related to synergistic effect of copper oxides active under visible light and AuCu presence [40]. Moreover, the photocurrent enhancement for the an-ACT electrode at + 1 V equals to $223 \mu\text{A cm}^{-2}$. Furthermore, the photopromoted catalysis of glycerine leads to the increase in current density for the n-ACT and the an-ACT materials. The proposed mechanism is shown in Scheme 2 [37, 38, 41].

The n-ACT electrode exhibits the photocurrent increase of $200 \mu\text{A cm}^{-2}$ registered in 0.1 M NaOH with 0.5 M glycerine at + 0.3 V versus Ag/AgCl/0.1 M KCl, whereas the an-ACT sample— $120 \mu\text{A cm}^{-2}$ (Table 1). However, higher photocurrent of $360 \mu\text{A cm}^{-2}$ was obtained at + 1 V for the AuCu

annealed nanomaterial and the current density at this potential was equal to ca. 3.3 mA cm^{-2} .

Figures 6 and 7 show the CV curves recorded in the solution of ethylene glycol and glycerine, respectively, and clearly the alcohol oxidation at the an-ACT electrode is observed. As it can be seen, in Figs. 6a and 7a with the increase in the scan rate the oxidation peak current density also grows up. A linear relationship between the peak current density and the square root of the scan rate was found up to 90 mV s^{-1} and 120 mV s^{-1} for GE and GLY, respectively (see Figs. 6b and 7b). The results indicate that the oxidation of GE and GLY is diffusion-controlled process [42]. However, it can be also stated that it is not a fully diffusion-controlled process due to the nonzero intercept of the equation [43]. According to Shahrokhian et al. [44], trimetallic Pt–Pd–Co/rGO nanomaterial exhibited dual linear region for the dependency of the anodic peak current density of ethylene oxidation versus scan rate with slopes equal to 812 mA cm^{-2} and 210 mA cm^{-2} . Dual behavior was ascribed to the decreasing rate of GE diffusion to electrode at higher scan rates. The measurements were performed from 0.2 mV/s to 600 mV/s [44]. According to Etesami et al. [43], the effect of scan rate on glycerol electrooxidation on the AuNPs/PG electrode showed increase in anodic peak with increasing scan rate up to 1000 mV/s with a slope of 2.1 mA/cm^2 . In the case of ethylene glycol for our materials, two peaks located at + 0.3 V and + 1 V show the same slope equals to $17 \mu\text{A cm}^{-2} \text{ mV}^{-1} \text{ s}$ in contrast to glycerine where 51 and $81 \mu\text{A cm}^{-2} \text{ mV}^{-1} \text{ s}$ were determined. The higher value of slope of a Randles–Sevcik (RDS) plot for glycerine in contrast to ethylene glycol can be correlated with the amount of hydroxyl groups—more hydroxyl groups the greater slope value. According to Khouchaf et al. [45], the peak

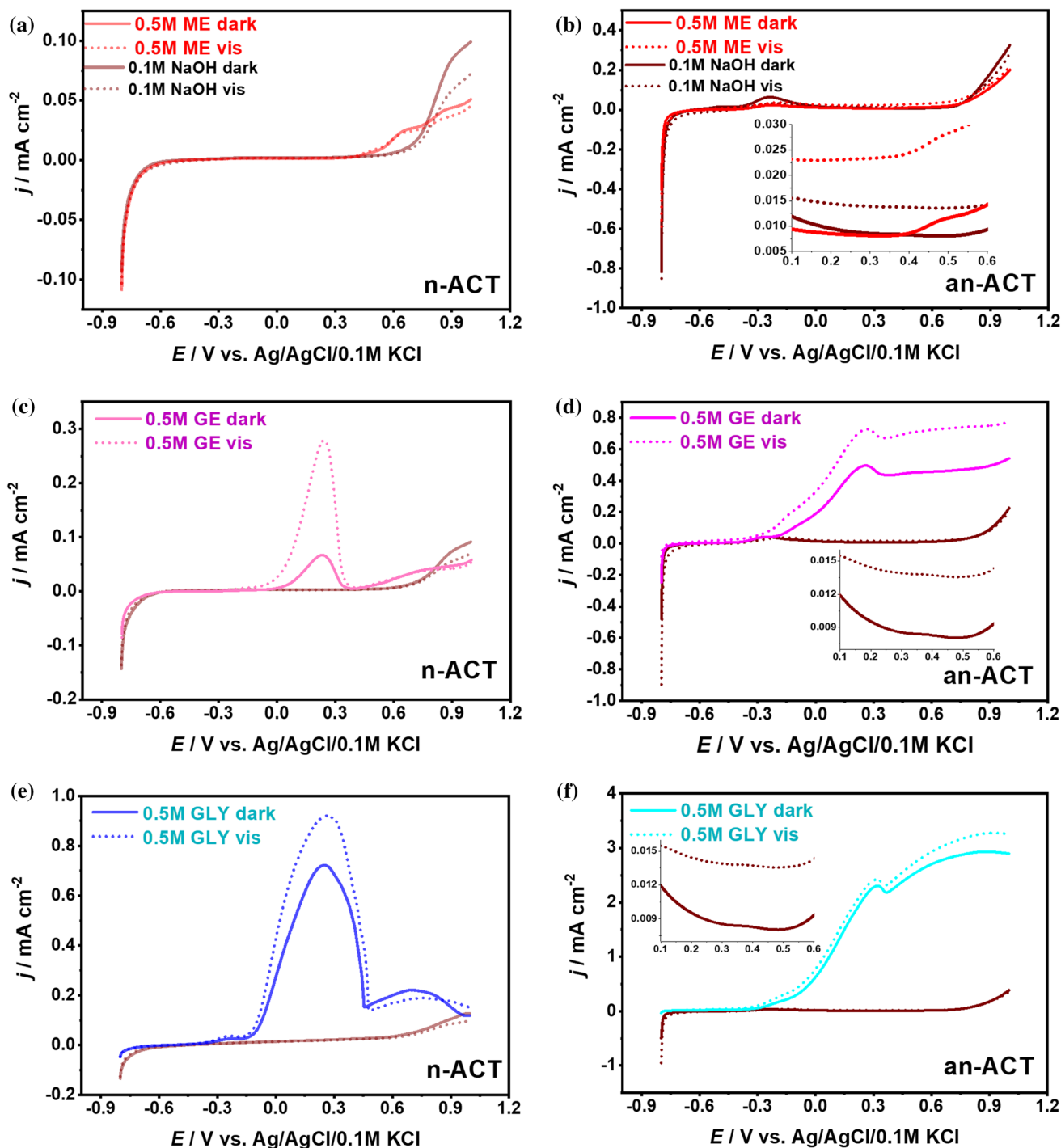


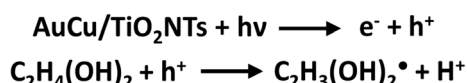
Figure 5 Linear voltammetry curves registered in 0.1 M NaOH without and with 0.5 M **a, b** methanol, **c, d** ethylene glycol and **e, f** glycerine for n-ACT and an-ACT electrodes in dark and under vis

located at c.a. 0.0 V versus $Ag/AgCl$ was attributed to $Cu/Cu(II)$ and $Cu(I)/Cu(II)$ oxidation process in alkaline solution, and also it was the potential of methanol oxidation. However, at the potential of +

illumination. (solid red—n-ACT 0.1 M NaOH dark, dotted red—n-ACT 0.1 M NaOH vis).

0.57 V, where $Cu(III)$ was formed in NaOH solution, higher anodic peak resulting from methanol oxidation was obtained. In our case, considering the glycerol containing electrolyte, one may assume that

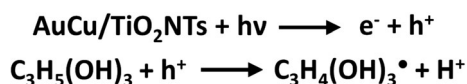
redox reaction involving high oxidation states of copper is replaced by GLY oxidation and the alcohol oxidation reaction is more promoted at + 1 V than at lower potentials (+ 0.3 V). Difference between C₂H₄(OH)₂ and C₃H₅(OH)₃ oxidation can be also caused by the interaction strength between the substrate and the adsorbate intermediates [30]. The interaction between the metal d states and the adsorbate states can be measured by density functional (DFT) calculations. As the scan rate exceeded



Scheme. 1 Oxidation reaction steps of ethylene glycol during material illumination.

Table 1 The photocurrent values for n-ACT and an-ACT electrode at + 0.3 V and + 1 V

	0.1 M NaOH + GE		0.1 M NaOH + GLY	
	$\Delta j/\mu\text{A cm}^{-2}$	E/V	$\Delta j/\mu\text{A cm}^{-2}$	E/V
n-ACT	210	+ 0.3	200	+ 0.3
an-ACT	230	+ 0.3	120	+ 0.3
	233	+ 1	360	+ 1



Scheme. 2 Oxidation reaction steps of glycerine during material illumination.

90 mV/s and 120 mV/s for glycol and glycerine, the current density approaches a plateau due to the reduction of the diffusion barrier resulting in the same concentration of alcohols in the solution and at the electrode surface.

Electrochemical impedance spectroscopy measurements were performed to obtain deeper insight into the electrical performance of the an-ACT electrode immersed in the solutions of different alcohols. The reaction not only depends on the applied potential but also on the availability of the charge carriers, therefore the experiments were carried out at the open circuit potential. Thus, the mechanism of reaction concerned charge transfer between solution and semiconductor as well as chemical bounds and compounds formed at the surface [46]. The Nyquist plots are shown in Fig. 8 while the equivalent electrical circuit used for fitting procedure ($R_E(\text{CPE}R_{CT}-W_O)$) is presented in Fig. 9.

The R_E element corresponds to the electrolyte resistance, the R_{CT} is the charge transfer resistance, the W_O is the Warburg open element and the CPE corresponds to the constant phase element. The impedance data obtained from Fig. 8 are listed in Tables 2 and 3. After immersion of the electrodes into the electrolyte their potentials have to compensate [47]. In the case of the semiconductor, it is Fermi level, whereas for the electrolyte—the chemical potential. If the Fermi level and the electrolyte potential are not equal, the electron transfer between them occurs. Schematic representation of energy levels and the possible charge transfer at the an-ACT

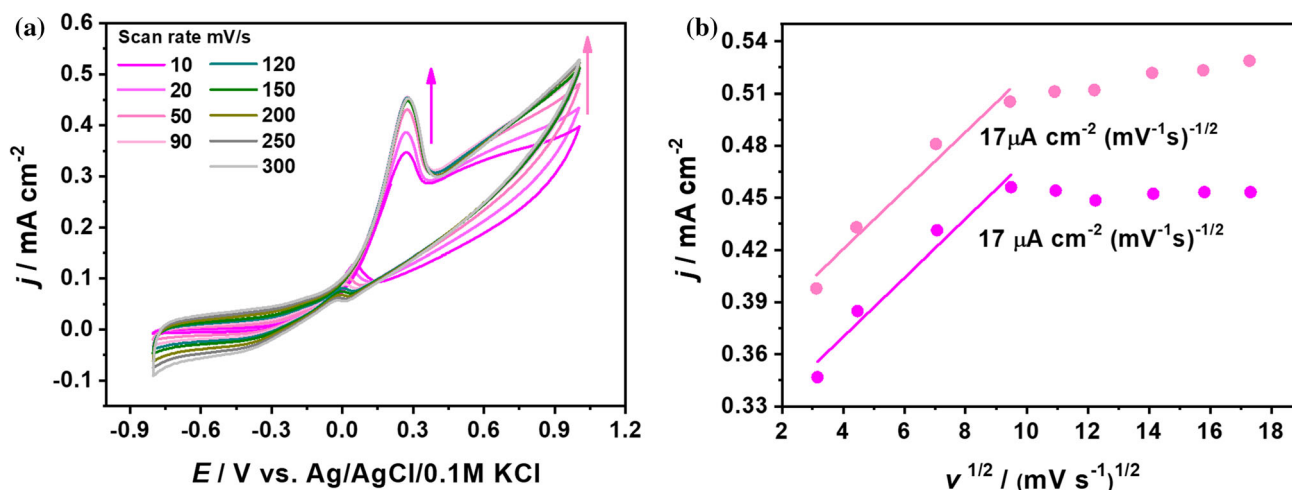


Figure 6 a CV curves of ethylene glycol oxidation at the an-ACT electrode at different scan rates in 0.1 M NaOH with 0.5 M GE solution and b corresponding calibration curves.

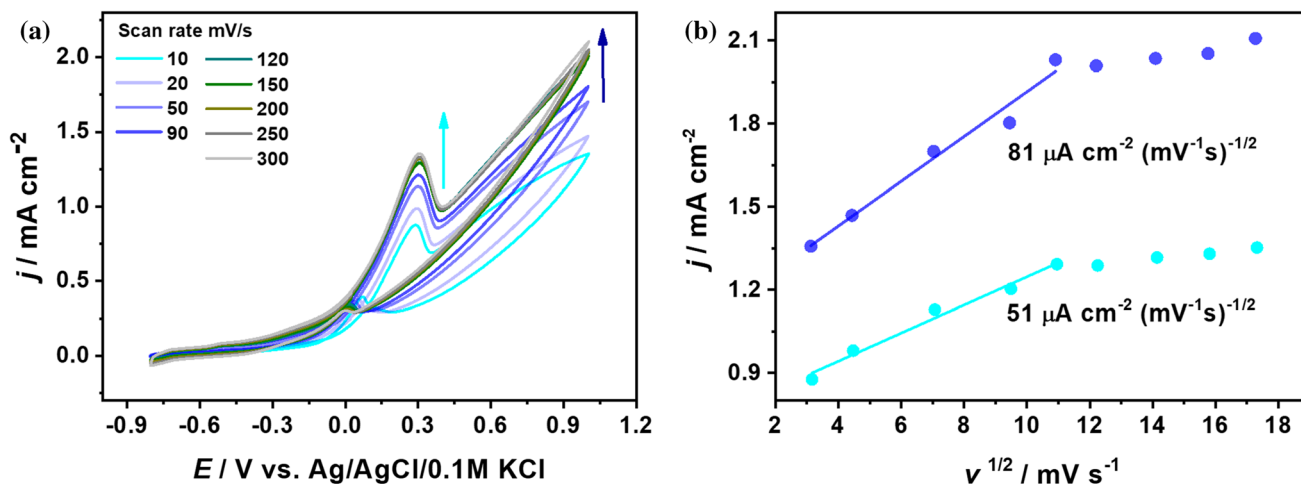


Figure 7 a CV curves of glycerine oxidation at the an-ACT electrode at different scan rates in 0.1 M NaOH with 0.5 M GLY solution and b corresponding calibration curves.

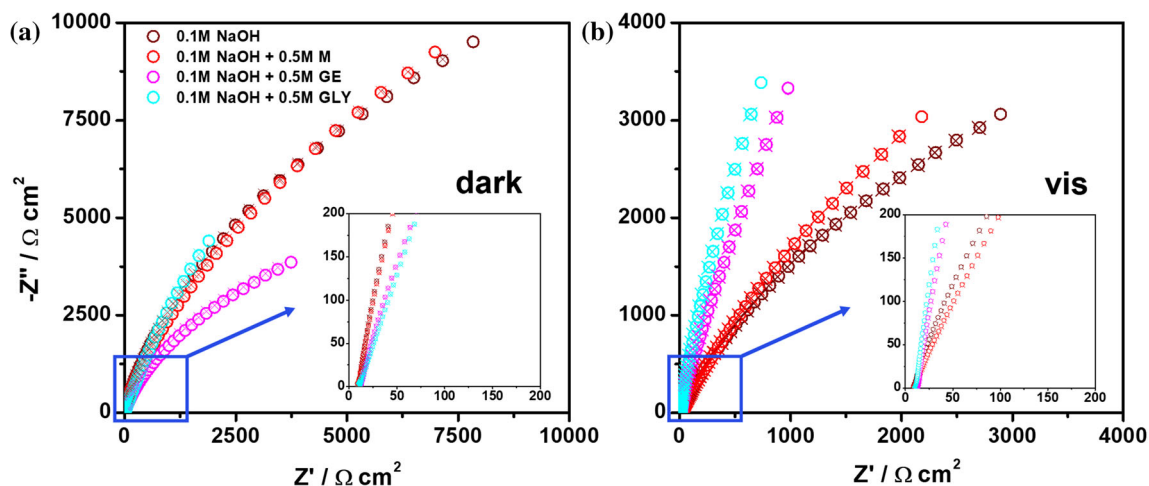


Figure 8 Impedance plots of the an-ACT electrode in methanol, ethylene glycol and glycerine solutions a in dark and b under vis light illumination.

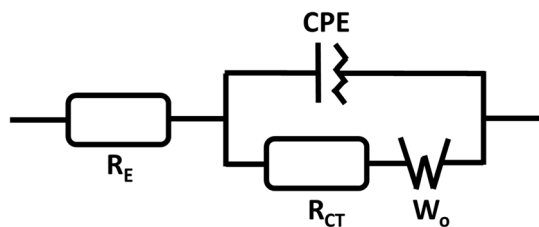


Figure 9 Model of the equivalent electrical circuit.

electrode/electrolyte interface is presented in Fig. 10. The values of potential presented in Fig. 10 above pink and blue bubbles correspond to the maximum of first alcohol oxidation peak on CV curves (Fig. 2).

Taking into account values of the ΔR_{CT} between samples resistance measured in the alkaline solution

without and with methanol, ethylene glycol or glycerine was equal to 200, 1000 and 1790 $\Omega \text{ cm}^{-2}$, respectively. However, the lowest value of R_{CT} equaled to ca. 10 $\Omega \text{ cm}^{-2}$ was measured for electrode immersed in glycerine solution. Such a small value of charge transfer resistance for GLY confirms the highly facilitated electron transfer between glycerine compound and electrode. These results can be correlated with the cyclic voltammetry scans where the highest current density was obtained for the glycerine oxidation. The decrease in the R_{CT} for all the electrodes under their illumination indicates their photoactivity, shift of the energy bands at the boundary of the electrode/electrolyte and a high mobility of carriers in TiO_2 [48]. Moreover, the

Table 2 Electrochemical impedance data for the an-ACT electrode carried out in methanol, ethylene glycol and glycerine solution in dark

Element	Unit	0.1 M NaOH	0.1 M NaOH + ME	0.1 M NaOH + GE	0.1 M NaOH + GLY
R_E	Ωcm^2	9.3	9.3	11.3	9.7
R_{CT}	Ωcm^2	1.8×10^4	1.6×10^4	0.8×10^4	10.2
Q	Fcm^{-2}	7.5×10^{-5}	7.9×10^{-5}	1.67×10^{-4}	2.92×10^{-4}
n		0.886	0.882	0.835	0.767
W_{or}	$\Omega\text{cm}^2 \text{ s}^{-1/2}$	41.7	305.6	13.5	288.3
W_{oc}	$\Omega\text{cm}^2 \text{ s}^{-1/2}$	0.0102	0.0594	0.0105	0.0112
χ^2		1.45×10^{-3}	1.84×10^{-3}	1.26×10^{-3}	7.34×10^{-4}

Table 3 Electrochemical impedance data for the an-ACT electrode carried out in methanol, ethylene glycol and glycerine solution under visible light illumination

Element	Unit	0.1 M NaOH	0.1 M NaOH + ME	0.1 M NaOH + GE	0.1 M NaOH + GLY
R_E	Ωcm^2	8.3	8.0	10.1	9.5
R_{CT}	Ωcm^2	0.6×10^4	5.6	1.2	0.5
Q	Fcm^{-2}	1.97×10^{-4}	3.53×10^{-4}	2.45×10^{-4}	2.54×10^{-4}
n		0.796	0.674	0.695	0.805
W_{or}	$\Omega\text{cm}^2 \text{ s}^{-1/2}$	6.2	10.4	149.9	124.2
W_{oc}	$\Omega\text{cm}^2 \text{ s}^{-1/2}$	0.0037	0.0003	0.0414	0.0337
χ^2		1.76×10^{-3}	1.24×10^{-3}	7.34×10^{-4}	7.36×10^{-4}

carriers' mobility is enhanced by the addition of alcohol to the electrolyte. As far as the constant phase element is concerned, it can be described by equation: $Z_{CPE} = 1/Q(j\omega)^n$ where Q is CPE parameter and n is CPE exponent with a value of $0 < n < 1$ [49]. In the case when the $n = 1$ the impedance corresponds to the pure capacitor, while for $n = 0$ the CPE is assigned to the resistor. The exponent n determines the surface heterogeneity, whereas Q is a quasi-capacitance of the electrode described as a double layer capacitance or a functionalized layer capacitance [50]. In our case the quasi-capacitance results from the absorbed hydroxyl groups of NaOH, methanol, ethylene glycol and glycerine on nanoparticles, while the heterogeneity originates from the alloy structure and the adsorption sites of alcohols and its coverage. For solid electrodes immersed in the electrolyte typical n value is in the range from 0.7 to 0.9 [51]. The influence of the position of hydroxyl groups of the dihydroxybenzene isomers on the adsorption mechanism was reported by Ryl et al. [52] Resorcinol, the compound containing two hydroxyl groups linked to the benzene ring, was characterized by impedance measurements and the best inhibitor efficiency at the high concentration equals to 100 mM in contrast to the ligand exchange model of adsorption for catechol

and quinol at lower concentrations (1 and 10 mM). According to Wysocka et al. [51] when the carboxylic acids corrosion inhibitors fully covered the electrode surface in the form of monolayer, the value of the homogeneity increased and resulted in increase in n values. Therefore, in our case there is a visible decrease in homogeneity along with the growing number of OH groups with simultaneous increase in a quasi-capacitance for experiments carried out in dark. The Warburg open element is attributed to the finite-length diffusion with refractive boundary ascribed by the equation:

$$Z_{W_o}(\omega) = \frac{W_{Or}}{\sqrt{\omega}}(1-j)\text{coth}\left[W_{Oc}\sqrt{j\omega}\right] \quad (4)$$

where W_{Or} is equal to Warburg coefficient and $W_{Oc} = d/D^{0.5}$ where d is the thickness of modified layer and D is the diffusion coefficient. The W_{Or} increases after methanol addition to the 0.1 M NaOH solution in dark as well as in light illumination. In the case of electrode immersed in the pure alkaline solution $\text{Cu}(\text{OH})_{\text{ads}}$ [53] and $\text{Au}(\text{OH})_{\text{ads}}$ [54] are formed on the surface. For the an-ACT sample in methanol solution, additional alcohol adsorption layer causes increase in the Warburg impedance. Furthermore, after light illumination in both cases, with and without methanol, decrease in W_{Or} and

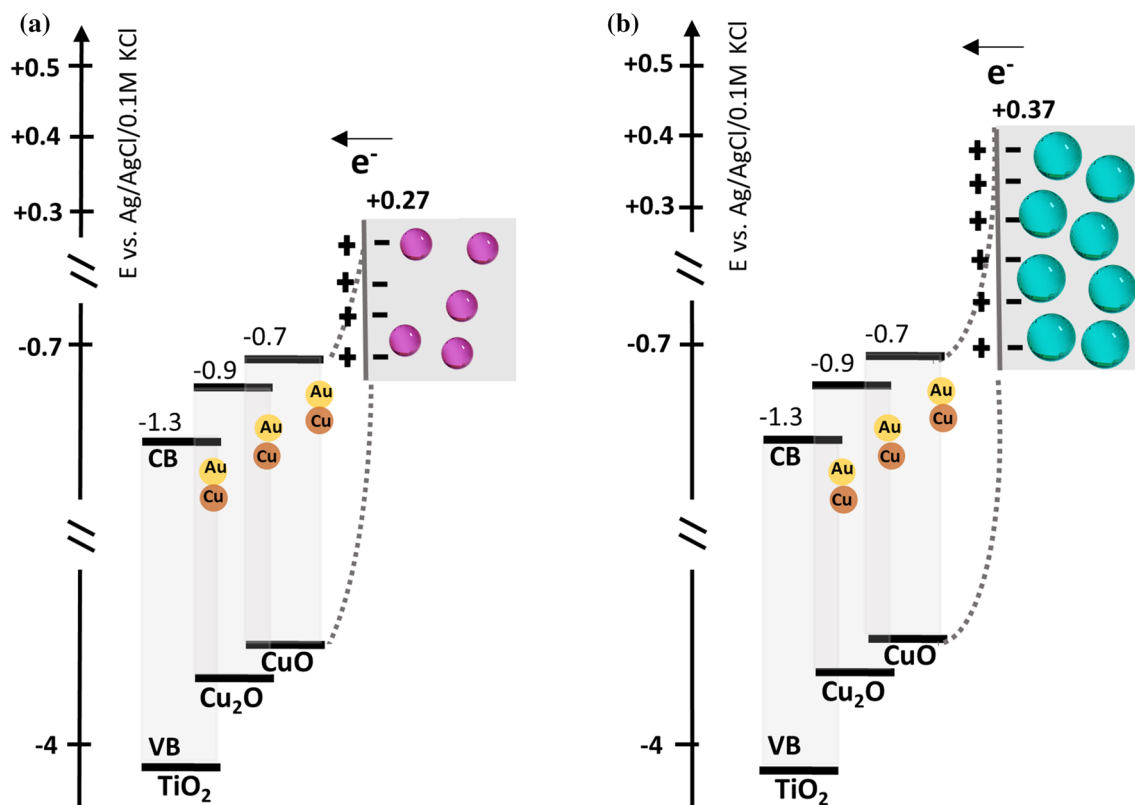


Figure 10 Schematic representation of energy levels and charge transfer for an-ACT electrode in dark in the solution of **a** ethylene glycol and **b** glycerine in 0.1 M NaOH.

W_{Oc} impedance takes place which can be attributed to the photoconductivity of material [55]. Other phenomena can be observed for samples measured in ethylene glycol and glycerine solution where not only alcohol adsorption layer and charge transfer under light illumination but also alcohol oxidation processes are taken into account. According to CV scans, at the OCP potential the beginning of glycol as well as glycerine oxidation, observed as current increase, can be seen, and therefore, not only $\text{Cu}(\text{OH})_{\text{ads}}$ and alcohol adsorption layer but also intermediates can be present at the electrode/electrolyte interface. The glycol oxidation process is slower than glycerine oxidation. The diffusion coefficient [56] of OH^- is higher for electrode immersed in ethylene glycol than in glycerine which can result in sparser layer at the electrode surface.

Conclusion

In this work, we presented detailed electrochemical results of catalytic active AuCu-modified TiO_2 nanotubes toward ethylene glycol and glycerine oxidation. The electrodes were fabricated via anodization of Ti, AuCu layer sputtering and rapid thermal treatment in an argon atmosphere which resulted in ordered TiO_2 nanostructure with spherical bimetallic nanoparticles. The prepared electrode material exhibited at + 0.3 V versus Ag/AgCl/0.1 M KCl ca. 20 times higher current density after glycol addition and 90 times after glycerine addition to the alkaline electrolyte. It should be highlighted that, annealed bimetallic structures are more catalytically active toward alcohol oxidation than non-annealed ones because of the increased number of Au and Cu active sites. Furthermore, AuCu-modified nanotubes exhibit enhancement of photocurrent under visible light illumination from photocatalytic alcohol oxidation caused by Cu_2O and CuO oxides presence. Moreover, pure titania nanotubes are not sensitive to ethylene glycol and glycerine. Additionally, rapid thermal

annealing in Ar atmosphere of bimetallic electrodes enhanced materials activity toward alcohol oxidation.

Acknowledgements

Research is financed by National Science Centre (Poland): Grant No. 2019/35/N/ST5/02604. KS and KG acknowledge the financial support of National Science Centre (Poland) via Grant No. 2017/26/E/ST5/00416.

Declarations

Conflict of interest The authors declare no competing financial interest.

References

- Guaitolini SVM, Yahyaoui I, Fardin JF, Encarnacao LF, Tadeo F (2018) A review of fuel cell and energy cogeneration technologies. 2018 9th International Renewable Energy Congress <https://doi.org/10.1109/irec.2018.8362573>
- Cassir M, Jones D, Ringuédé A, Lair V (2013) Electrochemical devices for energy: fuel cells and electrolytic cells. Handbook of Membrane Reactors 553–606. <https://doi.org/10.1533/9780857097347.3.553>
- Malik FR, Tieqing Z, Kim YB (2020) Temperature and hydrogen flow rate controls of diesel autothermal reformer for 3.6 kW PEM fuel cell system with autoignition delay time analysis. Int J Hydrogen Energy 45:29345–29355. <https://doi.org/10.1016/j.ijhydene.2020.07.20>
- Tu B, Yin Y, Zhang F, Su X, Lyu X, Cheng M (2020) High performance of direct methane-fuelled solid oxide fuel cell with samarium modified nickel-based anode. Int J Hydrogen Energy 45:27587–27596. <https://doi.org/10.1016/j.ijhydene.2020.07.07>
- Bambagioni V, Bevilacqua M, Bianchini C, Filippi J, Marchionni A, Vizza F, Wang LQ, Shen PK (2010) Ethylene glycol electrooxidation on smooth and nanostructured pd electrodes in alkaline media. Fuel Cells 10:582–590. <https://doi.org/10.1002/fuce.200900120>
- Peera SG, Lee TG, Sahu AK (2019) Pt-rare earth metal alloy/metal oxide catalysts for oxygen reduction and alcohol oxidation reactions: an Overview. Sustain Energy Fuels 3:1866–1891. <https://doi.org/10.1039/c9se00082h>
- Kannan R, Kim AR, Yoo DJ (2014) Enhanced electrooxidation of methanol, ethylene glycol, glycerol, and xylitol over a polypyrrole/manganese oxyhydroxide/palladium nanocomposite electrode. J Appl Electrochem 44:893–902. <https://doi.org/10.1007/s10800-014-0706-y>
- Kaur A, Kaur G, Singh PP, Kaushal S (2021) Supported bimetallic nanoparticles as anode catalysts for direct methanol fuel cells: a review. Int J Hydrogen Energy 46:15820–15849. <https://doi.org/10.1016/j.ijhydene.2021.02.037>
- Marelli M, Jouve A, Villa A, Psaro R, Balerna A, Prati L, Evangelisti C (2019) Hybrid Au-CuO nanoparticles: effect of structural features for selective benzyl alcohol oxidation. J Phys Chem C 123:2861–2871. <https://doi.org/10.1021/acs.jpcc.8b09449>
- Xu H, Yan B, Wang J, Zhang K, Li S, Xiong Z, Yang P (2017) Self-supported porous 2D AuCu triangular nanoprisms as model electrocatalysts for ethylene glycol and glycerol oxidation. J Mater Chem A 5:15932–15939. <https://doi.org/10.1039/c7ta04598k>
- Guo W, Yao X, Peng L, Lin B, Kang Y, Gan L (2020) Platinum monolayers stabilized on dealloyed AuCu core-shell nanoparticles for improved activity and stability on methanol oxidation reaction. Chin Chem Lett 31:836–840. <https://doi.org/10.1016/j.cclet.2019.06.018>
- Zhan W, Wang J, Wang H, Zhang J, Liu X, Zhang P, Chi M, Guo Y, Lu G, Sun S, Dan S, Zhu H (2017) Crystal structural effect of auct alloy nanoparticles on catalytic CO oxidation. J Am Chem Soc 139:8846–8854. <https://doi.org/10.1021/jacs.7b01784>
- Wang N, Han Y, Xu Y, Gao C, Cao X (2014) Detection of H₂O₂ at the nanomolar level by electrode modified with ultrathin AuCu nanowires. Anal Chem 87:457–463. <https://doi.org/10.1021/ac502682n>
- Sobczak I, Wolski Ł (2015) Au–Cu on Nb₂O₅ and Nb/MCF supports – Surface properties and catalytic activity in glycerol and methanol oxidation. Catal Today 254:72–82. <https://doi.org/10.1016/j.cattod.2014.10.051>
- Biswas R, Singh S, Ahmed I, Patil RA, Ma YR, Halder KK (2021) Rational design of Bimetallic Au/Cu nanostructure: an efficient catalyst for methanol oxidation. ChemNanoMat 7:158–164. <https://doi.org/10.1002/cnma.202000578>
- Palacio R, López D, Hernández D (2019) Bimetallic AuCu nanoparticles supported on CeO₂ as selective catalysts for glycerol conversion to lactic acid in aqueous basic medium. J Nanopart Res 21(7):1–3. <https://doi.org/10.1007/s11051-019-4594-2>
- Schünemann S, Dodekatos G, Tüysüz H (2015) Mesoporous silica supported Au and AuCu nanoparticles for surface plasmon driven glycerol oxidation. Chem Mater 27:7743–7750. <https://doi.org/10.1021/acs.chemmater.5b03520>

- [18] Chen B, Li X, Zheng R, Chen R, Sun X (2017) Bimetallic (Au–Cu core)@(ceria shell) nanotubes for photocatalytic oxidation of benzyl alcohol: improved reactivity by Cu. *J Mater Chem A* 5:13382–13391. <https://doi.org/10.1039/c7ta02047c>
- [19] Kim D, Xie C, Becknell N, Yu Y, Karamad M, Chan K, Crumlin EJ, Norskov JK, Yang P (2017) Electrochemical activation of CO₂ through atomic ordering transformations of AuCu nanoparticles. *J Am Chem Soc* 139:8329–8336. <https://doi.org/10.1021/jacs.7b03516>
- [20] Suzuki S, Tomita Y, Kuwabata S, Torimoto T (2015) Synthesis of alloy AuCu nanoparticles with the L10 structure in an ionic liquid using sputter deposition. *Dalton Trans* 44:4186–4194. <https://doi.org/10.1039/c4dt03557g>
- [21] Nguyen NT, Altomare M, Yoo J, Schmuki P (2015) Efficient photocatalytic H₂ evolution: controlled dewetting-dealloying to fabricate site-selective high-activity nanoporous Au particles on highly ordered TiO₂Nanotube arrays. *Adv Mater* 27:3208–3215. <https://doi.org/10.1002/adma.201500742>
- [22] Lipińska W, Grochowska K, Ryl J, Karczewski J, Siuzdak K (2021) Influence of annealing atmosphere on photoelectrochemical activity of TiO₂ nanotubes modified with AuCu nanoparticles. *ACS Appl Mater Interfaces* 13:52967–52977. <https://doi.org/10.1021/acsami.1c16271>
- [23] Martins CA, Ibrahim OA, Pei P, Kjeang E (2018) Towards a fuel-flexible direct alcohol microfluidic fuel cell with flow-through porous electrodes: assessment of methanol, ethylene glycol and glycerol fuels. *Electrochim Acta* 271:537–543. <https://doi.org/10.1016/j.electacta.2018.03.197>
- [24] Bhunia K, Khilari S, Pradhan D (2018) Monodispersed PtPdNi trimetallic nanoparticles-integrated reduced graphene oxide hybrid platform for direct alcohol fuel cell. *ACS Sustain Chem Eng* 6:7769–7778. <https://doi.org/10.1021/acssuschemeng.8b00721>
- [25] Xu H, Yan B, Zhang K, Wang J, Li S, Wang C, Shiraishi Y, Du Y, Yang P (2017) Ultrasonic-assisted synthesis of N-doped graphene-supported binary PdAu nanoflowers for enhanced electro-oxidation of ethylene glycol and glycerol. *Electrochim Acta* 245:227–236. <https://doi.org/10.1016/j.electacta.2017.05.146>
- [26] Fashedemi OO, Miller HA, Marchionni A, Vizza F, Ozoemena KI (2015) Electro-oxidation of ethylene glycol and glycerol at palladium-decorated FeCo@Fe core-shell nanocatalysts for alkaline direct alcohol fuel cells: functionalized MWCNT supports and impact on product selectivity. *J Mater Chem A* 3:7145–7156. <https://doi.org/10.1039/c5ta00076a>
- [27] Ozoemena KI (2016) Nanostructured platinum-free electrocatalysts in alkaline direct alcohol fuel cells: catalyst design, principles and applications. *RSC Adv* 6:89523–89550. <https://doi.org/10.1039/c6ra15057h>
- [28] Bao Y, Liu H, Liu Z, Wang F, Feng L (2020) Pd/FeP catalyst engineering via thermal annealing for improved formic acid electrochemical oxidation. *Appl Catal B* 274:119106. <https://doi.org/10.1016/j.apcatb.2020.119106>
- [29] Bagheri S, Muhd Julkapli N, Bee Abd Hamid S (2014) Titanium dioxide as a catalyst support in heterogeneous catalysis. *Sci World J* 2014:1–21. <https://doi.org/10.1155/2014/727496>
- [30] Fashedemi OO, Ozoemena KI (2014) Comparative electrocatalytic oxidation of ethanol, ethylene glycol and glycerol in alkaline medium at Pd-decorated FeCo@Fe/C core-shell nanocatalysts. *Electrochim Acta* 128:279–286. <https://doi.org/10.1016/j.electacta.2013.10.194>
- [31] Panjiara D, Pramanik H (2019) Electrooxidation study of glycerol on synthesized anode electrocatalysts Pd/C and Pd-Pt/C in a Y-shaped membraneless air-breathing microfluidic fuel cell for power generation. *Ionics* 26:2435–2452. <https://doi.org/10.1007/s11581-019-03385-8>
- [32] Houache MSE, Cossar E, Ntais S, Baranova EA (2018) Electrochemical modification of nickel surfaces for efficient glycerol electrooxidation. *J Power Sources* 375:310–319. <https://doi.org/10.1016/j.jpowsour.2017.08.089>
- [33] Lipińska W, Grochowska K, Karczewski J, Ryl J, Cenian A, Siuzdak K (2020) Thermally tuneable optical and electrochemical properties of Au-Cu nanomosaic formed over the host titanium dimples. *Chem Eng J* 399:125673–125685. <https://doi.org/10.1016/j.cej.2020.125673>
- [34] Liu S, Sun Z, Liu Q, Wu L, Huang Y, Yao T, Zhang J, Hu T, Ge M, Hu F, Xie Z, Pan G, Wei S (2014) Unidirectional thermal diffusion in bimetallic Cu@Au nanoparticles. *ACS Nano* 8:1886–1892. <https://doi.org/10.1021/nn4063825>
- [35] Böhme A, Sterl F, Kath E, Ubl M, Manninen V, Giessen H (2019) Electrochemistry on inverse copper nanoantennas: active plasmonic devices with extraordinarily large resonance shift. *ACS Photonics* 6:1863–1868. <https://doi.org/10.1021/acsp Photonics.9b00716>
- [36] Giri SD, Sarkar A (2016) Electrochemical study of bulk and monolayer copper in alkaline solution. *J Electrochem Soc* 163:H252–H259
- [37] Rajeshwar K (2007) Fundamentals of semiconductor electrochemistry and photoelectrochemistry. In: Bard AJ, Stratmann M, Licht S (eds) *Semiconductor electrodes and photoelectrochemistry*
- [38] Liu J, Fan C, Xie X, Jiang L (2021) Recent progress on photo-promoted alcohol electro-oxidation for fuel cells. *Energ Technol* 9:2000842–2000873. <https://doi.org/10.1002/ente.202000842>

- [39] Xu H, Song P, Fernandez C, Wang J, Zhu M, Shiraishi Y, Du Y (2018) Sophisticated construction of binary PdPb alloy nanocubes as robust electrocatalysts toward ethylene glycol and glycerol oxidation. *ACS Appl Mater Interfaces* 10:12659–12665. <https://doi.org/10.1021/acsami.8b00532>
- [40] Song P, Xu H, Wang J, Shiraishi Y, Du Y (2018) Construct 3D networked Au-Cu nanowires for enhanced plasmon-driven catalytic ethylene glycol oxidation through visible light irradiation. *J Power Sources* 399:59–65. <https://doi.org/10.1016/j.jpowsour.2018.07.0>
- [41] Wang H, Gao H, Zhai Ch, He Z, Yuan Ch, Zhu M (2020) Newly found photoactivated Pt anchored on three-dimensional layered WS₂/Carbon cloth for highly efficient ethylene glycol electro-oxidation. *Ind Eng Chem Res* 59:19252–19259. <https://doi.org/10.1021/acs.iecr.0c03436>
- [42] Campton RG, Batchelor-McAuley Ch, Dickinson EJF (2019) Understanding voltammetry: problems and solutions, vol 7. Imperial College Press, pp 128–129
- [43] Etesami M, Mohamed N (2011) Catalytic application of gold nanoparticles electrodeposited by fast scan cyclic voltammetry to glycerol electrooxidation in alkaline electrolyte. *Int J Electrochem Sci* 6:4676–4689
- [44] Shahrokhian S, Rezaee S (2017) Fabrication of trimetallic Pt–Pd–Co porous nanostructures on reduced graphene oxide by galvanic replacement: application to electrocatalytic oxidation of ethylene glycol. *Electroanalysis* 29:2591–2601. <https://doi.org/10.1002/elan.201700355>
- [45] Khouchaf A, Takky D, El Mahi CM, Benmokhtar S (2016) Electrocatalytic oxidation of methanol on glassy carbon electrode modified by metal ions (Copper and Nickel) dispersed into polyaniline film. *J Mater Sci Chem Eng* 4:97–105. <https://doi.org/10.4236/msce.2016.42011>
- [46] Lebedev MV (2020) Modification of the atomic and electronic structure of III–V semiconductor surfaces at interfaces with electrolyte solutions (Review). *Semiconductors* 54(7):699–741. <https://doi.org/10.1134/S1063782620070064>
- [47] Gerischer H, Ekardt W (1983) Fermi levels in electrolytes and the absolute scale of redox potentials. *Appl Phys Lett* 43:393–395. <https://doi.org/10.1063/1.94356>
- [48] Coy E, Siuzdak K, Pavlenko M, Załęski K, Graniel O, Ziółek M, Balme S, Miele P, Weber M, Bechelany M, Iat-sunskyi I (2020) Enhancing photocatalytic performance and solar absorption by schottky nanodiodes heterojunctions in mechanically resilient palladium coated TiO₂/Si nanopillars by atomic layer deposition. *Chem Eng J* 392:123702–123723. <https://doi.org/10.1016/j.cej.2019.123702>
- [49] Córdoba-Torres P (2017) Relationship between constant-phase element (CPE) parameters and physical properties of films with a distributed resistivity. *Electrochim Acta* 225:592–604. <https://doi.org/10.1016/j.electacta.2016.12.087>
- [50] Lipińska W, Ryl J, Slepski P, Siuzdak K, Grochowska K (2021) Exploring multi-step glucose oxidation kinetics at GOx-functionalized nanotextured gold surfaces with differential impedimetric technique. *Measurement* 174:109015–109026. <https://doi.org/10.1016/j.measurement.2021.109015>
- [51] Wysocka J, Cieslik M, Krakowiak S, Ryl J (2018) Carboxylic acids as efficient corrosion inhibitors of aluminium alloys in alkaline media. *Electrochim Acta* 289:175–192. <https://doi.org/10.1016/j.electacta.2018.08.070>
- [52] Ryl J, Brodowski M, Kowalski M, Lipinska W, Niedzialkowski P, Wysocka J (2019) Corrosion inhibition mechanism and efficiency differentiation of dihydroxybenzene isomers towards aluminum alloy 5754 in alkaline media. *Materials* 12:3067–3087. <https://doi.org/10.3390/ma12193067>
- [53] Kunze J, Maurice V, Klein LH, Strehblow HH, Marcus P (2003) In situ STM study of the effect of chlorides on the initial stages of anodic oxidation of Cu(111) in alkaline solutions. *Electrochim Acta* 48:1157–1167. [https://doi.org/10.1016/s0013-4686\(02\)00826-5](https://doi.org/10.1016/s0013-4686(02)00826-5)
- [54] Liu Z, Huang L, Zhang L, Ma H, Ding Y (2009) Electrocatalytic oxidation of d-glucose at nanoporous Au and Au–Ag alloy electrodes in alkaline aqueous solutions. *Electrochim Acta* 54:7286–7293. <https://doi.org/10.1016/j.electacta.2009.07.0>
- [55] Liu Z, Pesic B, Raja KS, Rangaraju RR, Misra M (2009) Hydrogen generation under sunlight by self ordered TiO₂ nanotube arrays. *Int J Hydrog Energy* 34:3250–3257. <https://doi.org/10.1016/j.ijhydene.2009.02.044>
- [56] Olejnik A, Karczewski J, Dołęga A, Siuzdak K, Grochowska K (2020) Novel approach to interference analysis of glucose sensing materials coated with Nafion. *Bioelectrochemistry* 135:107575–107586. <https://doi.org/10.1016/j.bioelechem.2020.107575>

Publisher's Note Springer Nature remains neutral with regard to jurisdictional claims in published maps and institutional affiliations.